J Comput Neurosci (2006) 21:131–151
DOI 10.1007/s10827-006-7863-x

The temporal structure of transient ON/OFF ganglion cell responses and its relation to intra-retinal processing

Andreas Thiel · Martin Greschner · Josef Ammermüller

Received: 2 November 2005 / Revised: 15 February 2006 / Accepted: 22 February 2006 / Published online: 26 May 2006

Abstract A subpopulation of transient ON/OFF ganglion cells in the turtle retina transmits changes in stimulus intensity as series of distinct spike events. The temporal structure of these event sequences depends systematically on the stimulus and thus carries information about the preceding intensity change. To study the spike events' intra-retinal origins, we performed extracellular ganglion cell recordings and simultaneous intracellular recordings from horizontal and amacrine cells. Based on these data, we developed a computational retina model, reproducing spike event patterns with realistic intensity dependence under various experimental conditions. The model's main features are negative feedback from sustained amacrine onto bipolar cells, and a two-step cascade of ganglion cell suppression via a slow and a fast transient amacrine cell. Pharmacologically blocking glycinergic transmission results in disappearance of the spike event sequence, an effect predicted by the model if a single connection, namely suppression of the fast by the slow transient amacrine cell, is weakened. We suggest that the slow transient amacrine cell is glycinergic, whereas the other types release GABA. Thus, the interplay of amacrine cell mediated inhibition is likely to induce distinct temporal structure in ganglion cell responses, forming the basis for a temporal code.

Action Editor: Jonathan D. Victor

A. Thiel (✉) · M. Greschner · J. Ammermüller
Neurobiology, Carl von Ossietzky University Oldenburg,
PO Box 2503, D-26111 Oldenburg, Germany
e-mail: andreas.thiel@uni-oldenburg.de

Keywords Retinal circuitry · Temporal coding · Amacrine cells · Glycine · Reciprocal feedback · Concatenated inhibition · Computational model

Introduction

Morphologically, physiologically, and neurochemically, amacrine cells form the largest variety of cell types in the vertebrate retina (Cajal, 1892; Morgan, 1992; Ammermüller and Kolb, 1996; MacNeil and Masland, 1998; Masland, 2001a). Amacrine cells are extensively involved in the intricate mesh of synaptic interactions in the inner plexiform layer (IPL), taking part in synaptic dyads postsynaptic to bipolar cells, reciprocal synapses back to bipolar cell terminals, serial synapses from amacrine to amacrine cells, and direct input to ganglion cells (Guiloff et al., 1988). Most amacrine cells seem to release GABA or glycine as a neurotransmitter, indicating that numerous combinations of inhibitory interactions take place in the IPL.

It is well accepted that the initially simple, spatially concentric receptive field organization of photoreceptors and bipolar cells is modified by a multitude of amacrine cell interactions. Especially in ganglion cells of non-mammalian retinae, this results in spatially complex receptive fields, responding for instance to orientation, motion or directionality (Marchiafava, 1979; Bowling, 1980; Granda and Fulbrook, 1989; Ammermüller et al., 1995; Dearworth and Granda, 2002).

In addition to these spatial aspects, amacrine cells shape the temporal structure of ganglion cell activity as well. For example, they appear to be essential for generating response transience from sustained activation evident at the bipolar cell level. Transient amacrine cell input was postulated to

play a major role in transient ON/OFF ganglion cell responses (Werblin and Dowling, 1969; Dowling, 1987; Sakai and Naka, 1987a, 1987b, 1988; Nirenberg and Meister, 1997; Roska et al., 1998), although conflicting results exist, indicating that other mechanisms may be at work as well (Golcich et al., 1990; Lukasiewicz et al., 1995; Awatramani and Slaughter, 2000). Models trying to explain response transience by synaptic interactions contain negative, possibly GABAergic feedback onto bipolar terminals, truncating transmitter release (Werblin et al., 1988; Maguire et al., 1989; Hennig et al., 2002), or a feedforward suppression of the postsynaptic ganglion cell (Toyoda et al., 1973; Miller and Dacheux, 1976; Miller, 1979). While the role of amacrine cells in the generation of basic ganglion cell response characteristics is still debated, it is well accepted that ganglion cell responses are shaped by transient and sustained inhibitory inputs (Werblin, 1977; Belgum et al., 1982, 1983; Lukasiewicz and Werblin, 1990). The transient inhibitory inputs appear to be glycinergic (Belgum et al., 1984), while sustained inhibitory inputs seem GABA-mediated (Werblin et al., 1988).

Temporally structured ganglion cell activity, termed "rhythmic" or "bursting", has been observed occasionally in mammalian and non-mammalian retinae (Schwartz, 1973; Ariel et al., 1983). Here, we report that after abrupt intensity changes a subpopulation of ON/OFF transient ganglion cells in the turtle retina elicits distinct sequences of action potentials. These sequences consist of two to three main spike events, each showing a characteristic, in some cases non-monotonic, latency dependence on the applied intensity change. Assuming that inner retinal amacrine cell interactions contribute massively to the emergence of these event sequences, we combined computational modeling and pharmacological interference to gain further insight into the physiological mechanisms leading to their generation.

Methods

Preparation and recordings

Electrophysiological measurements were done in 12 turtle *(Pseudemys scripta elegans)* retinae. Animals were sacrificed according to the guidelines of the University of Oldenburg Ethical Commitee and to ECC rules (86/609/ECC). Measurements were performed on isolated retinae with pigment epithelium attached. Retinae were constantly superfused with turtle ringer (120 mM NaCl, 5 mM KCl, 2 mM $CaCl_2$, 2 mM $MgCl_2$, 10 mM Glucose, 22 mM $NaHCO_3$, bubbled with 95% O_2/5% CO_2; pH 7.4). In the experiments that analyze effects of blocking glycinergic transmission, 75 μM strychnine was added to the Ringer solution.

Ganglion cell activity was recorded extracellularly with a 100-electrode silicon array (Cyberkinetics, Foxborough, MA) inserted from the pigment epithelium side into the ganglion cell layer. The Bionic 100-channel neural signal acquisition system (Cyberkinetics, Foxborough, MA) was used for amplifying, thresholding and storing the extracellular spike data. Simultaneously, intracellular recordings of horizontal or amacrine cells were performed using 3 M KCl filled borosilicate glass microelectrodes connected to an intracellular amplifier (npi SEC 1L/H). Penetration with the microelectrodes was done from the ganglion cell side. Intracellular signals were displayed on an oscilloscope screen and stored for offline analysis (Powerlab, ADInstruments Pty Ltd.,CO). Horizontal and amacrine cell responses were identified according to their characteristic waveforms and depth of the recording electrode in the retina. Horizontal cell responses also served as control for the viability of this preparation. Time courses, amplitudes, and receptive field profiles (tested with centered spots of increasing size) of the horizontal cell responses were indistinguishable from those obtained in previous recordings from the turtle eyecup preparation. Measurements of cone photoreceptor responses were performed separately. No reliable intracellular recordings could be done during slow flicker stimulation since these stimulation protocols lasted too long.

Typically, each electrode of the multielectrode array recorded the activity of more than one cell and therefore several spike waveforms occurred at a single electrode. We used the supervised k-means clustering software SpikeSorter (Cyberkinetics, Foxborough, MA) for separation of spike waveforms. We selected only those electrodes that had waveforms typical of single-unit activity, which were unequivocal in terms of both amplitude and shape and showed a clear refractory period in the interspike interval histogram. In general, well separable multi-prototype signals were obtained from 20–60 electrodes. Since the electrode distance of our array is 400 μm, the recording of one cell on more than one electrode is almost excluded. After spike separation, the time stamps of first threshold crossings were stored as a temporal sequence for each unit. These time stamps were used for further analysis.

Light stimulation

Retinae were stimulated with spatially homogeneous, full field light flashes and with pseudo-random full field intensity steps (flicker) applied to the ganglion cell side. Maximum retinal illuminance was 1000 lx. Flashes were applied every 2 s and lasted for 200 ms, except for the photoreceptor recordings, where flash duration was 500 ms. In the pseudo-random intensity step paradigm, intensity was abruptly switched to a new level every 1000 ms, leading to slow flicker stimulation. Light flashes allow for a physiological

classification of the intracellularly recorded cells and for comparison with previous data, whereas the pseudo-random intensity steps minimize adaptation effects and cover more intensity combinations. Stimulus sequences were generated in such a way that all possible transitions from both the maximum and the minimum intensity level to every intermediate level occurred equally often, but in random order.

Stimulation was done via an optical bench using a white LED as the light source (Luxeon, San Jose, CA), controlled by a standalone programmable microprocessor, which allowed for very precise timing. Stimulus intensity was chosen from a set of dual logarithmic levels: intensity at each level is twice as high as the one on the level directly below. The number of levels was between 10 in the flash paradigm and 16 in the flicker stimulation. Thus, intensity ranges were between 3 and 4.8 log units, covering the whole sensitivity spectrum of the recorded cells from detection limit up to saturation. The distribution of intensities chosen here is similar to the one found in natural images, since intensities in natural environments show a roughly symmetric distribution on a logarithmic scale, covering a range of 2.5–3 log units (van Hateren, 1997). On a linear scale, this is equivalent to a higher fraction of lower intensities with a long tail at the high intensity end.

In order to obtain a compact representation and for easier comparison with the flash data, stimuli and corresponding responses in the flicker paradigm were sorted according to four different conditions. For this, start and end intensities were defined as those intensities present before and after an intensity transition, respectively. Sorting was done as follows: From a cell's complete spike train, slices of 250 ms duration were selected, beginning at the time stamps of all those transitions that share the minimum intensity as their start. This condition is termed "ON—start intensity fixed". All spike train slices selected were then ordered systematically according to the steps' end intensities and plotted as spike rasters (see e.g. Fig. 4). This was also done for intensity steps starting with various lower intensities, but all jumping to the highest intensity. Spike train slices of this second condition also report responses to intensity increases, and are termed "ON—end intensity fixed". The third condition consists of steps all jumping to the lowest intensity. This necessarily yields responses to intensity decreases, thereby constituting the third condition, called "OFF—end intensity fixed". Finally, the fourth condition is the one combining all transitions with the maximum intensity as their start, this is termed "OFF—start intensity fixed". The first and the third condition correspond to the light ON and light OFF phase of the flash stimulation. In the figures, the four transition conditions are symbolized by grayscale images next to the raster plots.

Cellular retina model

General remarks

The computational retina model was implemented using the Interactive Data Language (IDL; Research Systems Inc., Boulder, CO). Due to the spatially homogeneous nature of the stimuli we used, only a single representative of each cell class is modeled (see Fig. 2 for a schematic overview of the model cells and their connectivity). Using a temporal integration step size of 1 ms, each model neuron's membrane potential $v(t)$ is computed by numerically integrating a passive membrane differential equation (Gaudiano, 1994):

$$\frac{dv(t)}{dt} = -A_v v(t) + d_v(t)(D_v - v(t)) - h_v(t)(H_v + v(t)), \quad (1)$$

with A_v denoting the passive membrane decay rate to resting potential in the dark, i. e. in the absence of input, D_v and H_v setting the saturation levels for depolarization and hyperpolarization respectively, and $d_v(t)$ and $h_v(t)$ indicating total depolarizing and total hyperpolarizing inputs. All parameters as well as the inputs in Eq. (1) are assumed to be non-negative.

Since the absolute value of the membrane potential in the dark is unknown for inner retinal cells, it is defined to be zero for the model neurons. Thus, positive excursions are interpreted as depolarizations, and negative excursions as hyperpolarizations. In the following equations, the depolarized and hyperpolarized portions of the membrane potential v are indicated by $v^+ := vH(v)$ and $v^- := v(1 - H(v))$ respectively, with $H(\cdot)$ denoting the Heaviside step function. Passing both v^+ as well as v^- to the postsynaptic cell represents synaptic transmission capable of positive and negative modulation around a basic level, as is the case for synapses that tonically release a certain amount of transmitter. On the other hand, weak transmission at resting level, which consequently cannot be further reduced, is easily modeled by including only positive signals v^+ into the postsynaptic neuron's membrane equation.

Several inputs converging onto the same neuron from different presynaptic cells could be modelled by including more additive terms with corresponding D_v and H_v values into Eq. (1). However, due to the lack of appropriate data, we used only a single depolarizing and a single hyperpolarizing term in each membrane equation. In case of multiple depolarizing or hyperpolarizing connections converging upon the same neuron, inputs are multiplied by individual connection strengths and then summed. Unless otherwise noted, D_v and H_v are fixed to 1 to reduce the number of the model's free parameters.

Photoreceptor

In each simulation time step t, light intensity relative to the experiment's maximum intensity is fed into the model as a numerical value $I_{rel}(t) \in [0, 1]$. Signal processing in the model photoreceptor (PR) starts by smoothing the sequence of intensities using a first order low-pass filter with time constant τ. The filtered signal *i(t)* is then transformed by a static saturating nonlinear function to yield sufficiently large responses for the whole range of input intensities. The nonlinearity is of the form

$$r(t) = R\left(\frac{i(t)}{i(t) + I_0}\right)^n, \tag{2}$$

with R determining the saturation level. To account for the fact that an intensity increase causes a hyperpolarization in the PR, R is chosen to be negative. I_0 denotes the input that yields the half maximum response, and n is a real number. Further smoothing of the signal due to the enzymatic light transduction cascade in the PR is represented by two additional low-pass filter stages, with their time constants τ being identical to the first filter. This yields the smoothed intensity signal $s(t)$.

The model photoreceptor's membrane dynamics $p(t)$ is described by

$$\begin{aligned}\frac{dp(t)}{dt} = & -A_p p(t) - W_p^h h^-(t - \Delta t_h)(D_p - p(t)) \\ & + s(t - \Delta t_s)(H_p + p(t)).\end{aligned} \tag{3}$$

Since we want the model PR to hyperpolarize in response to intensity increases, we include the smoothed intensity signal $s(t–\Delta t_s)$ as a hyperpolarizing input in Eq. (3). This signal is slightly delayed by Δt_s to ensure the correct response latency. In addition to $s(t–\Delta t_s)$, the PR also receives delayed depolarizing input $h^-(t–\Delta t_h)$ from the model horizontal cell. This input is weighted by the synaptic strength parameter W_p^h, with the subscript p indicating the photoreceptor as the target cell of the connection, and the superscript h denoting horizontal cell as the signal source. Horizontal cell depolarizations h^+ are omitted as an input signal in Eq. (3) because the model horizontal cell does not depolarize (see below). Since both $h^-(t)$ and $s(t)$ are negative, signs of the second and third parts of the equation are inverted compared to Eq. (1). The saturation variables D_p and H_p were adjusted by error minimization as described below.

Horizontal cell

The membrane potential *h(t)* of the model horizontal cell (HC) is computed according to

$$\begin{aligned}\frac{dh(t)}{dt} = & -A_h h(t) + W_h^p\, p^+(t)(D_h - h(t)) \\ & + W_h^p\, p^-(t)(H_h + h(t)).\end{aligned} \tag{4}$$

Saturation values D_h and H_h were both fixed. Setting $D_h = 0$ avoids depolarization of the model HC, in accordance with our experimental observations. Since the synapse between PR and HC transmits both the PR's depolarization and its hyperpolarization (Normann and Perlman, 1979b), p^+ as well as p^- occur in Eq. (4), even though the effect of p^+ is negligible: its peak amplitude is small compared to the peak amplitude of p^-, and is even further reduced in the model by the fact that $D_h = 0$.

For the sake of clarity, the complete differential equations describing the potential dynamics are omitted in the following. Instead, only the inputs $d_v(t)$ and $h_v(t)$ to the model neurons are given.

Bipolar cells

To obtain membrane depolarizations during intensity increases, the first type of bipolar cell (ON BC) receives sign inverted input from the PR. Therefore, the PR hyperpolarization $p^-(t - \Delta t_{ON})$ appears as a depolarizing input to the ON BC and vice versa:

$$\begin{aligned} d_{b\,ON}(t) &= -W_b^p\, p^-(t - \Delta t_{ON}) - W_{b\,ON}^{a\,S\,ON}\, a_{S\,ON}^-(t) \\ h_{b\,ON}(t) &= W_b^p\, p^+(t - \Delta t_{ON}) + W_{b\,ON}^{a\,S\,ON}\, a_{S\,ON}^+(t). \end{aligned} \tag{5}$$

The PR signal is delayed here to represent the fact that signal transmission from PRs is slower due to the metabotropic receptors of ON BCs' compared to the OFF BCs' ionotropic receptors. In addition to the PR, the ON BC is also coupled to an amacrine cell with sustained response characteristics, the activation of which is described by $a_{S\,ON}(t)$. This amacrine cell is depolarized by increasing intensities (see below) and acts inhibitorily on the ON BC's potential, which requires its positive part to be added to the hyperpolarizing input of the ON BC. The effect of p^+ is again small, like for the horizontal cell. However, this is not the case for $a_{S\,ON}^-$. This part of the input is essential to quickly reduce the ON BC's potential down to its resting level after light offset, thereby avoiding undesirable long lasting depolarizations.

In a symmetric way, the model bipolar cell which hyperpolarizes in response to light increases (OFF BC) receives sign conserved input from the PR, delayed by an ionotropic receptor time lag Δt_{OFF}, and inhibitory input $a_{SOFF}(t)$ from a sustained OFF amacrine cell:

$$\begin{aligned} d_{b\,OFF}(t) &= W_b^p\, p^+(t - \Delta t_{OFF}) - W_{b\,OFF}^{a\,S\,OFF}\, a_{S\,OFF}^-(t) \\ h_{b\,OFF}(t) &= -W_b^p\, p^-(t - \Delta t_{OFF}) + W_{b\,OFF}^{a\,S\,OFF}\, a_{S\,OFF}^+(t) \end{aligned} \tag{6}$$

Amacrine cells

The model's sustained ON amacrine cell (ON AC_{su}) receives input $b_{ON}(t)$ exclusively from the ON BC. Like for the BCs, adding the hyperpolarizing input b^-_{ON} is essential here to ensure a fast return to resting level after light offset:

$$\begin{aligned} d_{a\,S\,ON}(t) &= W^b_{a\,S}\, b^+_{ON}(t) \\ h_{a\,S\,ON}(t) &= -W^b_{a\,S}\, b^-_{ON}(t)\,. \end{aligned} \tag{7}$$

The sustained OFF amacrine cell (OFF AC_{su}) correspondingly is coupled to the OFF BC:

$$\begin{aligned} d_{a\,S\,OFF}(t) &= W^b_{a\,S}\, b^+_{OFF}(t) \\ h_{a\,S\,OFF}(t) &= -W^b_{a\,S}\, b^-_{OFF}(t)\,. \end{aligned} \tag{8}$$

The sustained ACs' saturation levels $H_{a\,S\,ON}$ and $D_{a\,S\,\mathrm{OFF}}$ needed to be reduced to 0.3 to avoid long lasting over- and undershoots.

The slow transient ON/OFF amacrine cell (ON/OFF AC_{str}) only receives depolarizing input, but from both the ON and the OFF BCs:

$$\begin{aligned} d_{a\,ST\,ONOFF}(t) &= W^{b\,ON}_{a\,ST\,ONOFF}\, b^+_{ON}(t) \\ &\quad + W^{b\,OFF}_{a\,ST\,ONOFF}\, b^+_{OFF}(t) \\ h_{a\,ST\,ONOFF}(t) &= 0. \end{aligned} \tag{9}$$

To minimize fluctuations in this cell's potential time course, saturation values are $D_{a\,ST\,ONOFF} = 0.03$ and $H_{aST\,ONOFF} = 0$. Furthermore, only depolarizations from both ON and OFF BCs occur as input signals. This is required in the model because as the ON BC depolarizes, the OFF BC simultaneously hyperpolarizes. Including b^-_{ON} and b^-_{OFF} would therefore result in an unwanted partial cancellation of the ON and OFF pathway signals.

The input to the fast transient ON/OFF amacrine cell (ON/OFF AC_{ftr}) is described by the following equations:

$$\begin{aligned} d_{a\,FT\,ONOFF}(t) &= W^{b\,ON}_{a\,FT\,ONOFF}\, b^+_{ON}(t) \\ &\quad + W^{b\,OFF}_{a\,FT\,ONOFF}\, b^+_{OFF}(t) \\ h_{a\,FT\,ONOFF}(t) &= W^{a\,ST\,ONOFF}_{a\,FT\,ONOFF}\, a^+_{ST\,ONOFF}(t)\,. \end{aligned} \tag{10}$$

Thus, this cell is depolarized by both ON and OFF BC inputs $b_{ON}(t)$ and $b_{OFF}(t)$ and hyperpolarized by the signal $a_{ST\,ONOFF}(t)$ from the slow transient ON/OFF amacrine cell. The ON/OFF AC_{ftr} only receives the depolarized parts of the bipolar cell signals for the same reason already described above for the slow transient AC. Since the latter is never hyperpolarized, $a^-_{ST\,ONOFF}$ is omitted from Eq. (10).

Ganglion cell

The model ganglion cell receives depolarizing inputs $b_{ON}(t)$ and $b_{OFF}(t)$ from both ON and OFF bipolar cells and hyperpolarizing input $a_{FT\;ONOFF}(t)$ from the fast transient ON/OFF amacrine cell:

$$\begin{aligned} d_g(t) &= W^{b\,ON}_g\, b^+_{ON}(t) + W^{bOFF}_g\, b^+_{OFF}(t) \\ h_g(t) &= W^{a\,FT\,ONOFF}_g\, a^+_{FT\,ONOFF}(t)\,. \end{aligned} \tag{11}$$

No hyperpolarizing BC input is included in Eq. (11). This is to prevent such signals from canceling the depolarization caused by the BC from the opposite pathway. Thus, ON and OFF bipolar inputs do not act in antagonistic fashion here, like proposed elsewhere (Gaudiano, 1994). Rather, they are necessary to describe the ON/OFF response characteristic of the ganglion cell type considered here. The fast transient amacrine cell provides temporally restricted inhibition during strong activation of the GC, while otherwise exerting no effect. Therefore, only the depolarized part $a^+_{FT\,\mathrm{ON\,OFF}}$ occurs in Eq. (11).

As a final step, action potentials are generated by the model GC on the basis of its membrane potential $g(t)$. To account for the fact that no spikes occur if the cell is not sufficiently depolarized, and to mimic the stochastic nature of spike generation, the value $f'(t) = G\,[g(t) - \theta]_+$ is interpreted as the basic firing probability. $[x]_+ := xH(x)$, thus denoting the positive part of x. The gain factor G scales the original signal $g(t)$ to generate an appropriate number of spikes, and θ is the firing threshold. However, since neurons are less likely to generate another action potential immediately after having elicited a spike, the probability in subsequent time steps needs to be reduced. This is accomplished here by subtracting from the basic signal $f'(t)$ a function that is largest immediately after the spike occurrence and decays exponentially towards zero with time constant τ_θ. Thus, during a simulation time step t, a spike is generated according to the modified probability $f(t)$:

$$f(t) = G\,[g(t) - \theta]_+ - F \sum_i H(t - t_i)\, e^{-(t-t_i)/\tau_\theta}, \tag{12}$$

with $t > t_i$ being the time stamps of previous spikes and $H(\cdot)$ again denoting the Heaviside function. In this way, the neuron gradually regains its original firing probability after a certain relative refractory period determined by the parameters F and τ_θ, similar to a dynamic threshold in some integrate and fire model neurons (Eckhorn et al., 1990).

Parameter adjustment

To fully describe all of the model neurons and their connectivity, 50 parameters need to be specified. This high number,

in connection with the feedback loops, delays and nonlinear operations contained, may result in very complex behavior. Furthermore, there exists the possibility of overfitting, i.e. describing different cells' responses or a single cell's response to different stimuli with very different parameter values. Therefore, we first reduced the number of free parameters. The effect that input from a presynaptic model neuron has on a postsynaptic neuron's membrane potential is determined by the combination of two factors, the connection's coupling strength W, and the corresponding saturation constant D_v or H_v. If one of these factors is fixed, the impact of presynaptic input can still be adjusted by changing the other one. Thus, it is sufficient to only adjust the coupling parameters while fixing the saturation constants D_v and H_v. Furthermore, in feedback loops, one of two parameters determining the reciprocal coupling strengths may be kept constant without loss of generality. Finally, the membrane decay rates A_{bOFF},$A_{aFTONOFF}$, and A_g were set to a fixed "fast" value of 500/s, since in these cells, smoothing the incoming activation may be omitted without compromising the quality of the reproductions. Having excluded the redundant parameters, 27 were left to be fitted.

Outer retinal parameters

The model parameters determining the PR's and HC's responses were adjusted first. As a reference, we used the membrane time courses of PR and HC potentials obtained by intracellular recordings during the flash experiments. We manually chose a set of parameters as a starting point. After that, the parameter set was further adjusted by minimizing the total absolute deviation between experimental and model potential traces, simultaneously for all intensities and for both neurons, with traces normalized to avoid different weighting due to differences in the cells' response amplitudes. Parameter adjustment was accomplished by applying the Downhill-Simplex method of Nelder and Mead for minimizing multidimensional functions (Flannery et al., 1993), implemented in IDL. We included into the error function the PR potential's deviation from zero after 1.8 s of darkness, thereby penalizing long lasting depolarizations of the PR after light offset. As mentioned above, the saturation values D_h and H_h were excluded from the fitting procedure, as well as the coupling strength W_p^h. All other 11 parameter values were subject to the adjustment process. To ensure a sufficient coverage of parameter space and to avoid having the optimization procedure get stuck in local minima, it was repeated 150 times, each time with the starting parameters randomized around those obtained by the qualitative manual procedure. Finally, we chose the parameter set which best fitted the experimental data with respect to a small error value as well as clearly displaying the main characteristics of the cells' responses.

Inner retinal and spike generation parameters

After an appropriate set of outer retinal parameter values was found, we kept those values fixed and next determined the bipolar, amacrine and ganglion cell parameters, including those of the spike generation process. This separation of inner and outer retinal parameters reduces the likelihood of overfitting. The elimination of free parameters described above left 12 inner retinal and four spike generation parameters to be adjusted. Like before, parameter search was started manually to find an initial set, and continued algorithmically afterwards. To this end, we minimized the error between a ganglion cell's spike trains obtained in flash experiments and the model reproduction, again simultaneously for all levels of intensity. We first generated a graded signal by convolving each trial of the spike data using a Gaussian function with a standard deviation of 7 ms, the result corresponding to the cell's instantaneous firing rate. This is necessary to ensure the error minimization algorithm's proper function, since two binary spike trains always yield a maximum error unless all spikes exactly coincide, the error function being insensitive to how close in time the spikes are. Using the total absolute deviation between the experimental instantaneous firing rates and their model counterparts as an error signal enabled us to determine a set of model parameters that reproduced the experimentally observed spike trains. Since we considered it an important part of the response, we additionally introduced a penalty term into the error function to ensure that the second spike event does not disappear from the model response during the fitting procedure.

Flicker and strychnine experiments

To reproduce the spiking behavior of ganglion cells during the flicker experiments, parameters were initially chosen identical to those obtained by fitting the model responses to data from the flash stimulation. Due to the differing adaptational states of the retina during the two types of experiments, some parameter modifications were necessary, although we tried to keep the number of altered parameters low to minimize overfitting effects. Since simulating responses to the flicker stimulus takes much longer compared to flash stimulation, parameter adjustment was done manually to avoid the large number of simulations needed for an algorithmic error minimization.

To appropriately reproduce the ganglion cell's behavior in the control condition of the strychnine experiment, parameters were slightly modified once more, starting from

the set chosen to model the flicker experiment. Again, the number of alterations was kept as small as possible. After a set of parameters was found, only the connection strength $W_{a\,FT\,ONOFF}^{a\,ST\,ONOFF}$ of slow to fast transient ON/OFF ACs was allowed to be varied to reproduce the spike event patterns after application of strychnine. For modeling the time course of gradually decreasing glycinergic coupling, we assumed an exponential function to describe the effect of applying strychnine continuously. The start and end values for this function are the two values of $W_{a\,FT\,ONOFF}^{a\,ST\,ONOFF}$ chosen to represent the control condition and the strongest strychnine effect respectively. The time constant of the exponential function was adjusted manually.

Spike train distance analysis

Naturally, the experimentally observed spikes do not occur at exactly the same times during repetitions of identical stimuli. We used this trial-to-trial variability as a measure to estimate the quality of our model reproductions. If spike trains elicited by the model are as similar to the experimental spike trains as the experimental spike trains are to each other, then the model reproduction may be regarded as sufficiently good. The similarity of spike trains can elegantly be expressed by the spike train distance metric D^{spike} introduced by Victor and Purpura (1996). Using this metric, we first determined the distances between experimental spike trains averaged over repetitions of identical intensity steps. This was done for both the flash and the flicker experiments. For the flash experiment, ON and OFF part were treated separately, corresponding to the first and the third condition of the flicker data. To obtain a single value for each condition, distance values for different intensities were averaged. For comparison with the model predictions, the procedure was repeated, this time computing the distances between the experimental and the model spike trains. In the following, the difference of the resulting two quantities, the average distance between experimental spike trains among themselves and the one between experimental and model spike trains, is expressed in terms of the standard deviation (sdv) of the experimental distance values.

Since here we are concerned with comparing the temporal structure of responses, the choice of the cost parameter q, which regulates the D^{spike} metric's temporal sensitivity, is crucial. We determined q's value as follows: First, artificial spike trains were generated, containing the same number of spikes as their experimental counterparts, but randomly distributed within intervals of the same duration. These synthetic responses thus lack any temporal structure. Now, a reasonable choice for q is the value that maximizes the difference between experimental spike trains and synthetic responses, emphasizing the temporally clustered nature of the former. The value found by this procedure is $q = 100$/s, yielding a difference value of 2.32 sdv between experimental and synthetic data. According to Victor and Purpura (1996), the reciprocal of q is a measure of the metric's temporal precision, or in other words, the time scale it is most sensitive to. The particular q-value chosen here corresponds to sensitivity on the scale of 20 ms, in accordance with the minimum separation of the spike events, which is of the same order of magnitude. Although a smaller value of q yields smaller average distance measures, distinction of separate events is blurred. On the other hand, larger q-values overemphasize spike timing, always resulting in large spike train distances unless responses are identical.

Results

Flash experiments

In a first series of experiments, we recorded ganglion cell (GC) action potentials in response to short full field light flashes superimposed on a dark background (Fig. 1). Simultaneously, intracellular recordings of horizontal or amacrine cells were performed. Thus, conditions were identical for both spike and intracellular recordings, enabling an exact comparison of the interneurons' response waveforms and spike timing in GCs.

Spike events as a function of intensity steps

The GCs investigated in this study generate action potentials both during short periods after the intensity increase at the beginning of the flash as well as after the intensity decrease at flash offset. In this respect, they are clearly fast, transient ON/OFF ganglion cells. In contrast to classical ON/OFF cells, however, they produce one or two short additional "bursts" of spikes that are obviously distinct from the initial responses, both after light onset and offset. Between bursts, essentially no spikes are elicited. This subpopulation of transient ON/OFF ganglion cells was regularly recorded in all retinae studied. Since the bursts often contain only one or two spikes, we will term them "events", in order to distinguish them from classical bursting behavior of other neurons, and in accordance with previous terminology (Berry et al., 1997). The various events are clearly visible as bands of spikes when responses to several stimulus repetitions are plotted one above another in spike raster plots, as has been done in the left column of Fig. 1 for three different stimulus intensities. While spikes within the same event are merely separated by the cells' refractory period of 3–4 ms, intervals between events are at least an order of magnitude larger. The temporal precision of spike generation evident in the spike rasters is especially noteworthy for those events that are not immediately preceded by the flash on- and offsets. These events lack sharp stimulus transients to be locked to, which

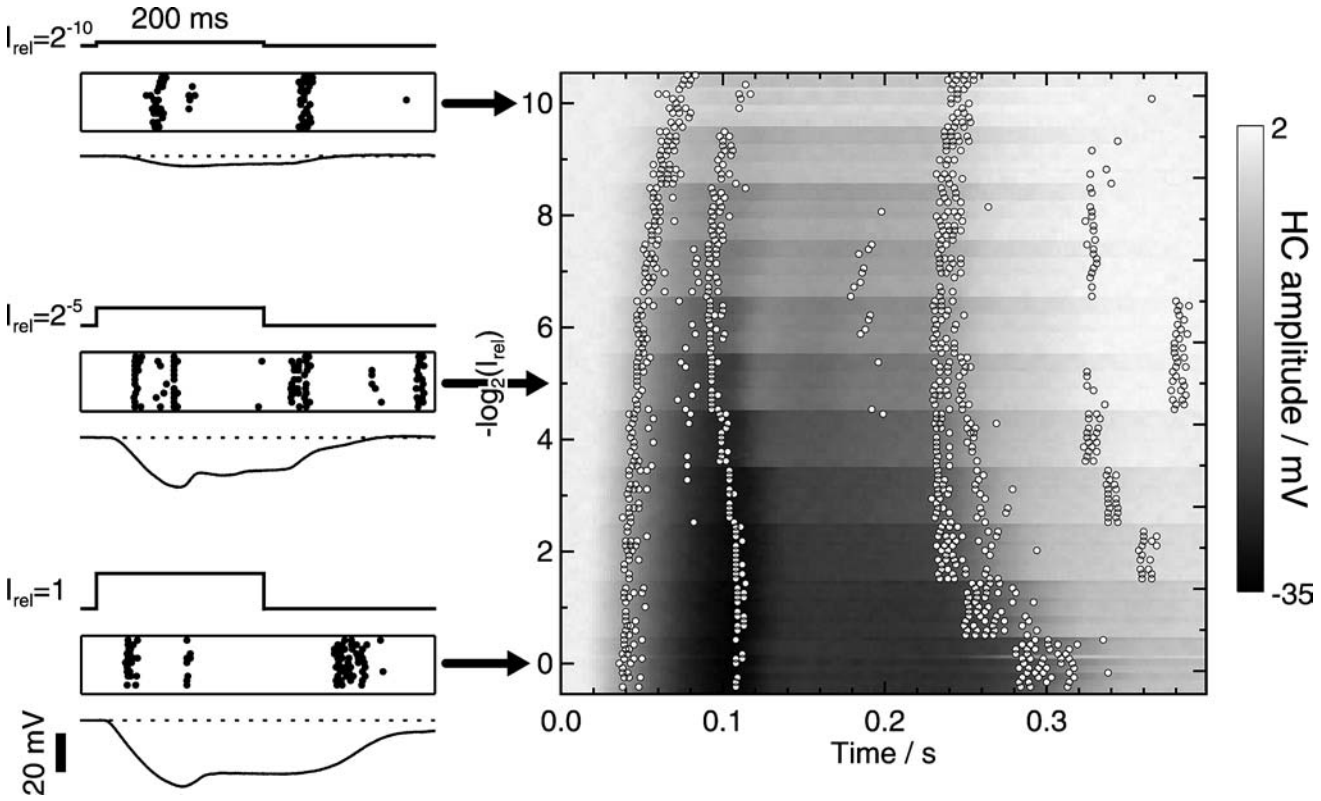

Fig. 1 Simultaneous response of a ganglion (GC) and a horizontal cell (HC) to full field light flashes of different intensities. *Left column*: Three raster plots of action potentials recorded from a GC during identical repetitions of a flash stimulus ($n = 12$). Stimulus intensity time course is symbolized above the rasters, with flash intensity I_{rel} measured relative to the maximum intensity noted at the left. The traces below the raster plots show the membrane potential time courses of a horizontal cell, recorded simultaneously to the GC spikes and averaged over trials ($n = 12$). *Right panel*: Overlay of GC spike trains and HC potentials for all intensities and stimulus repetitions. Responses to repetitions of the same stimulus conditions are plotted directly above one another, and these sub-rasters are in turn arranged according to the relative light intensity I_{rel} of the flashes. Intensity increases from top to bottom. HC membrane potential is shown as grayscale background, with dark shading indicating strong hyperpolarization

is generally considered a prerequisite for high temporal precision in spike timing (Mainen and Sejnowski, 1995).

The latency of the events, i.e. the time of their occurrence relative to stimulus onset, depends on flash intensity. The gradual change of the various events' latencies as a function of flash intensity can best be observed if spike trains in response to flashes of increasing intensity are plotted below each other in a single raster plot (Fig. 1, right panel). The first event's latency decreases monotonically with increasing flash intensity from approximately 75 ms after the onset of the darkest flash down to 40 ms for the brightest flashes. This classical decrease of latency with increasing intensity is in accordance with previous observations (Sestokas et al., 1991). Surprisingly, however, the second event does not simply copy its predecessor's behavior. While its latency decreases during the transition from low to intermediate intensities (latencies 110 ms at $I_{rel} = 2^{-10}$ vs. 90 ms at $I_{rel} = 2^{-5}$), it grows when stimulation intensity further increases from intermediate to high (latency 110 ms at $I_{rel} = 2^{0}$), resulting in a characteristic spike raster resembling the letter 's'.

The OFF part of the response also consists of more than one event, although the second and third of those events cannot be clearly traced across all different intensities in the example of Fig. 1. The first OFF event displays a behavior similar to the second ON event, in the sense that its latency, measured from flash offset, first decreases from around 50 ms to 30 ms and then increases up to approximately 100 ms with increasing intensity. The exact shape of the spike raster, however, is different from the second ON event's s-shape and rather resembles the form of the letter 'c'.

Horizontal cell membrane potential time course

In order to reveal intra-retinal mechanisms leading to the emergence of the temporal event patterns and their characteristic intensity dependence, we analyzed the flash responses of retinal interneurons. In the left column of Fig. 1, the voltage traces of a horizontal cell (HC) recorded simultaneously to the ganglion cell are shown for three example intensities, whereas in the right panel of Fig. 1, the horizontal cell

responses are transferred to a grayscale image underlying the ganglion cell spike pattern.

Initial slope and peak hyperpolarization of the HC potential first become larger with increasing intensity, then saturate at high intensities. After the peak hyperpolarization, the HC membrane is partly repolarized, then stays at a plateau and completely repolarizes slowly after offset of the light stimulus. The spikes of the first ON and the first OFF event occur preferentially at those times where the HC response displays steep slopes. This indicates that the overall behavior of the spike event patterns is shaped by the responses of outer retinal cells. However, the subsequent events both in the ON and the OFF response do not seem to follow the HC potential so clearly. We therefore suggest that it is necessary to consider processes in the inner retina as well to explain the characteristics of these additional events.

Cellular retina model

General remarks

The computational retina model was developed with the intention of clarifying the mechanisms leading to the observed spike event patterns by reproducing main aspects of intraretinal processing. Figure 2 gives a schematic overview of all model neurons and their connectivity. All major retinal cell classes were taken into account, including different types of amacrine cells. Furthermore, the ON/OFF response characteristic observed in the ganglion cells requires both an ON and an OFF pathway, with the signals from both pathways finally converging onto the same GC. On the other hand, the model should of course be minimal in the sense that it reproduces the observed response behavior with as few cellular mechanisms as possible. Since in this study we are concerned with temporal processing, spatially homogeneous stimuli were chosen in order to avoid complications with spatial aspects. Therefore, only a single cell of each class is modeled, assuming that neurons in neighboring parts of the retina form identical modules, receive an identical input and thus behave the same. The model photoreceptor (PR) receives as its input the time course of the relative light intensities. All model neurons' membrane potentials are then computed sequentially for each simulation time step, taking into account the neurons' previous states and input arriving from connected cells (see Methods for details on the model implementation).

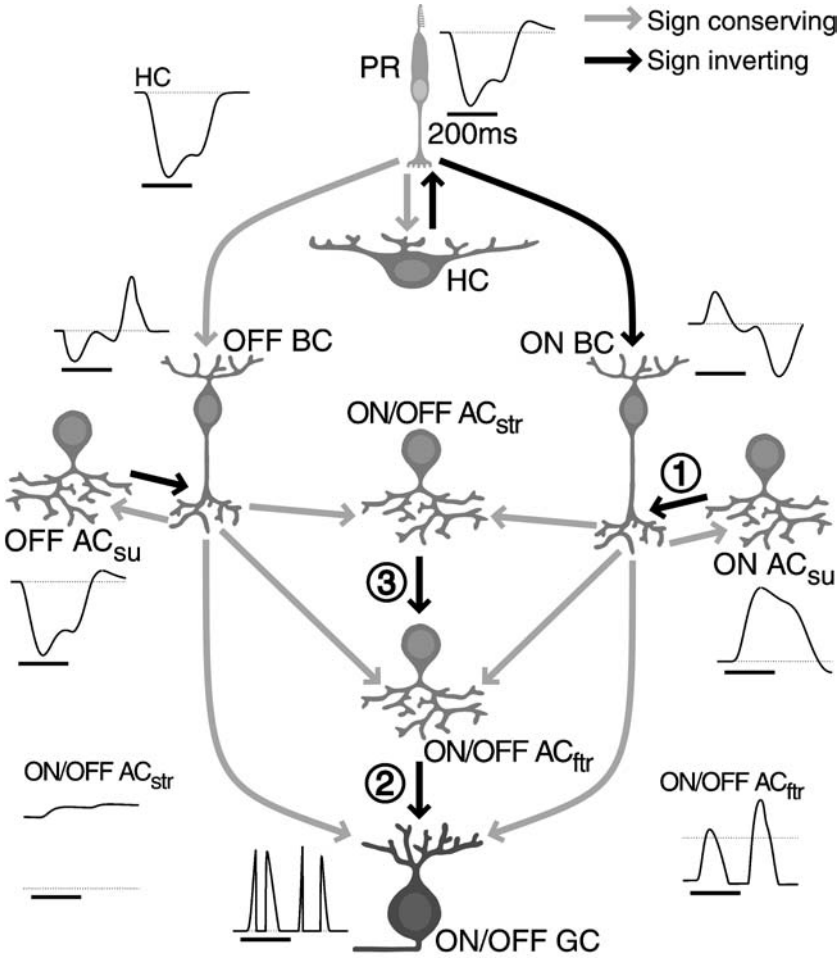

Fig. 2 Schematic drawing of the cellular retina model showing the cell types modeled and their connectivity. Arrows drawn in black indicate sign inverting connections, while light gray arrows indicate sign conserving connections. Model potential time courses in response to a 200 ms flash of intermediate intensity $I_{rel} = 2^{-5}$ are shown as black traces in the cells' vicinity. Dotted horizontal lines indicate each cell's dark resting potential, thick horizontal lines below the traces represent stimulus duration. Encircled numbers mark connections that could possibly be affected by the glycine antagonist strychnine (see section "Effects of strychnine application")

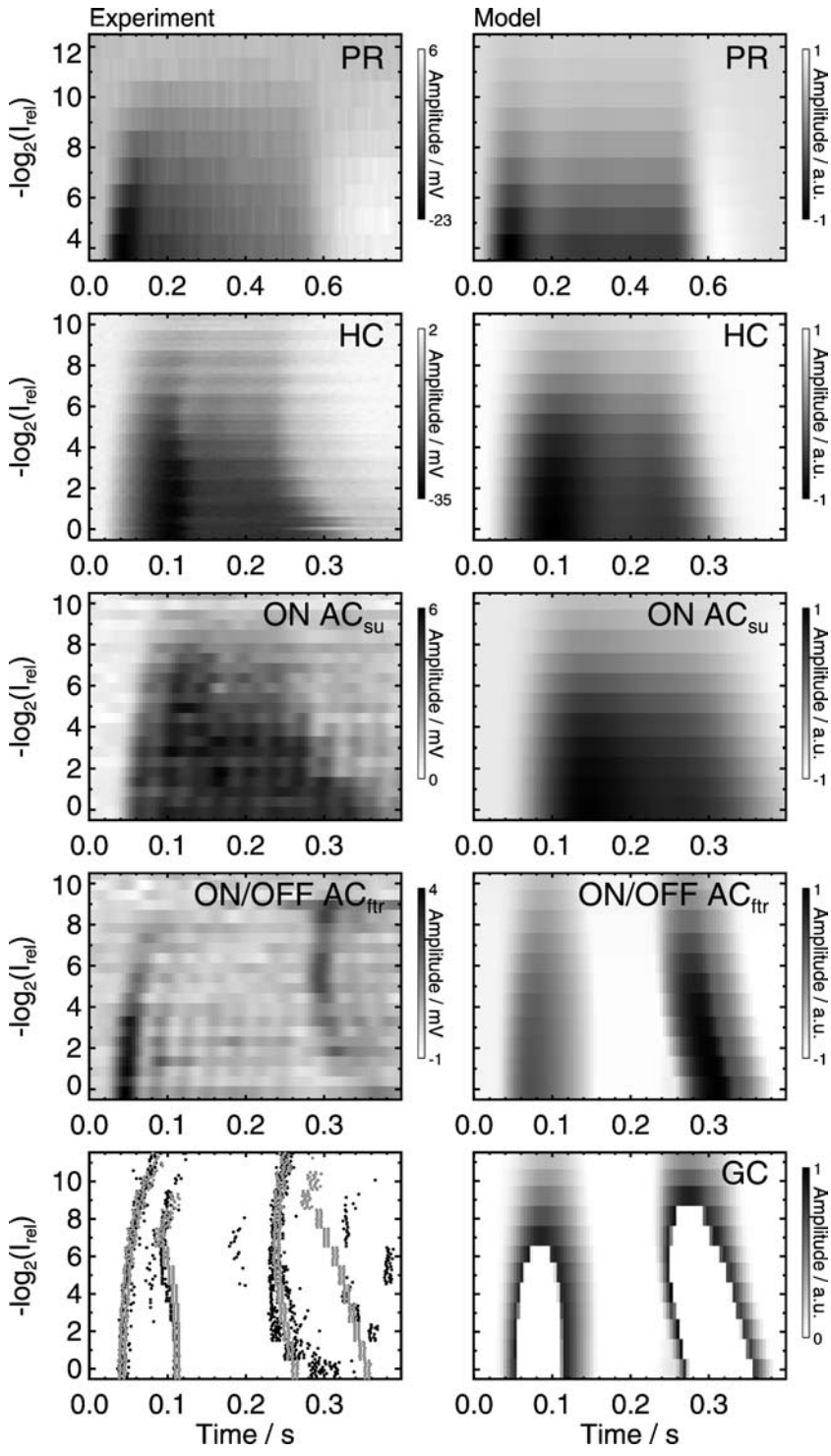

Fig. 3 Intracellular potentials and spike trains for the flash stimulation paradigm. *Left column:* experimental data, *right column:* model predictions. Cell type is indicated in the upper right of the panels. Note the reversal of the colormaps for the amacrine cells (AC) and ganglion cell (GC), indicating depolarization with light increase in contrast to hyperpolarization in the photoreceptor (PR) and horizontal cell (HC). Time 0.0 indicates stimulus onset, stimulus offset is at 0.5 s in the PR data and at 0.2 s elsewhere. The bottom left panel shows both experimental (black dots) and model (gray dots) spike rasters, plotted together on top of each other for easier comparison of the timing of spike events

Modeling cells in the outer retina

The model for outer retinal processing consists of a cone photoreceptor and a horizontal cell which are mutually connected. Both are hyperpolarized by increases in intensity. Experimental results as well as model reproductions of PR and HC potential time courses are shown as a function of flash intensity in the two top rows of Fig. 3. To reproduce the correct peak hyperpolarization in both cells for the complete range of input intensities, it is necessary to compress the input range by a saturating nonlinearity before further processing (Eq. (2)). The intensity signal is additionally filtered by three low-pass stages, corresponding to the enzymatic cascade of light transduction taking place inside the PR

(reviews: Müller and Kaupp, 1998; Burns and Lamb, 2003; for a model, see Hennig and Funke, 2001). This filtering reproduces the smooth time course of hyperpolarization seen in the data. It is the first prerequisite for the latency behavior observed in the ganglion cell spike timing. Although intensity is increased instantaneously at flash onset, already at this stage different input intensities are transformed into more or less steep time courses of hyperpolarization. These differences in the initial membrane potential slopes then yield different spike latencies due to the threshold of spike initiation in the ganglion cells.

The OFF response's c-shape is also essentially set up in the outer retina. It is determined by the previous intensity level, the smooth return to baseline after stimulus offset, and the nonlinear transformation. Time courses after high intensity transitions are compressed more strongly by the saturating nonlinearity, leading to a shallower slope and therefore an increased latency compared to intermediate transitions. On the other hand, low intensity stimulation leads to small amplitudes and consequently to shallower slopes as well, which also prolongs the latency. The shape of the OFF response is a reflection of both mechanisms, resulting in a non-monotonic latency dependence with a minimum at intermediate intensities.

The time course of the model HC potential essentially follows that of the PR, with an additional stage of mild filtering due to its membrane's low-pass properties. The initial transient repolarization of the PR is caused by delayed HC feedback, which in turn affects the HC, reproducing the characteristic initial transient before the plateau hyperpolarization is reached. By minimizing the difference between the data traces and the model computations, it was possible to determine a set of parameters for the combination of model PR and HC that satisfactorily reproduced both cells' initial slope of hyperpolarization, its peak value, the plateau potential and the overall response duration for all intensities (see Table 1 for the final outer retinal parameter values).

Modeling transient bipolar cell responses

Next, we intended to generate a transient activation in the model bipolar cell that is depolarized by intensity increases (ON BC), lasting approximately until the second ON event observed in the ganglion cells. Passing only this BC signal to the GC, it is possible to restrict spikes after stimulus onset to a period of approximately 100 ms, thus including both the first and second ON event. The interruption of spiking activity between these events is then generated in a second step described below.

The PR potential remains hyperpolarized as long as the light stimulus continues. Thus, if this sustained activity would be passed unaltered to GCs via bipolars, the GCs would respond with a series of spikes also lasting during the whole 200 ms long period of light stimulation. For the fast transient GC type considered here, this is obviously not the case. As mentioned above, experimental evidence has been gathered in support of amacrine cell feedback onto BC terminals shaping GCs' transient response characteristics. We therefore introduced into the model a negative feedback loop acting on the BC via a depolarizing sustained amacrine cell (ON AC_{su}). This mechanism truncates the BC response after around 100 ms following light onset. The model amacrine cell's membrane time constant is large, allowing for the initial part of the PR response to be passed until the AC is sufficiently depolarized. This results in a BC depolarization that inherits the intensity dependent latency of the PR, while its overall duration increases with increasing intensity, determined by the time constant of the sustained AC and strength of its feedback signal. The third row of Fig. 3 shows the membrane potential traces of the model sustained AC next to a corresponding, experimentally obtained recording of a sustained ON amacrine cell that shows the same long lasting depolarization.

To reproduce the ON/OFF nature of the ganglion cell responses we included a second type of bipolar cell (OFF BC), which receives PR signals without sign inversion, and is therefore hyperpolarized by light increases. The model GC's offset response is a consequence of depolarizing input originating from this OFF BC. By a mechanism of delayed negative feedback symmetric to the one just described for the ON pathway, the OFF BC itself responds with a transient hyperpolarization at the beginning of the light stimulus, but also with a transient depolarization at light offset (inset in Fig. 2, OFF BC). This offset depolarization is caused by an ongoing inhibition from the sustained OFF AC, while the PR input is already diminishing.

Creating the pause between spike events

Having shaped the overall duration of the BC and therefore also the GC response by the negative feedback of sustained ACs, we next sought to identify a possible mechanism that is responsible for the pause in spike activity between the first and the second event. A simple refractory period is not appropriate, since this results in a second event that is shaped in the same way as the first, with monotonic changes in latency rather than an s-shaped intensity dependence. Inhibiting GCs by a temporally delayed or smoothed version of the BC activity would also not generate the correct non-monotonic dependency. Instead, it looks as if an inhibitory process suppresses GC activity after the first event's spikes, creating a dip in the GC membrane time course, but releases its inhibition immediately before the transient ON signal from the BC dies off, allowing for the second spike event. This proposed inhibition needs to display the same intensity dependence as the BC's transient ON signal, namely a decreasing latency

and an increasing duration with increasing intensity. If, on the other hand, it starts a little later and lasts slightly less long, it would be appropriate to reduce GC depolarization during the pause and allow it to be converted into spikes only at its beginning and end. We therefore included a neuron into the model that receives excitatory input from both ON and OFF BCs and acts inhibitorily onto the GC if depolarized. This cell has to be interpreted as an amacrine cell, since the only direct, inhibitory GABAergic or glycinergic input to GCs originates from ACs (Morgan, 1992). Corresponding to its input, this cell displays a fast transient ON/OFF response pattern, which is shown in the fourth row of Fig. 3 and the inset of Fig. 2 (ON/OFF AC_{ftr}). The existence of this type of amacrine cell is confirmed by our intracellular recordings, showing fast transient amacrine cell responses with depolarization both at the increase as well as the decrease of light intensity (fourth row of Fig. 3). The model ON/OFF AC_{ftr} potential traces agree qualitatively, although the response to the offset of high intensity flashes is stronger in the model than in the experimental recordings.

However, to fulfill the above-mentioned requirements, the fast transient AC has to be inhibited itself, since otherwise it would completely abolish the GC depolarization, not just the part between the two ON events. Thus, a third type of amacrine cell is needed. This one is also depolarized by ON and OFF BC depolarizations, but in the model has a very large membrane time constant, resulting in an almost constant activation and a slow, small and sluggish depolarizing response both at light ON and OFF. Therefore, it resembles some slow transient amacrine cells (ON/OFF AC_{str}) from the literature (Marchiafava and Weiler, 1982; Ammermüller and Kolb, 1995). Its output is transmitted to the fast transient AC, lowering this cell's membrane potential and thereby limiting its suppression of the GC to the period in between the two ON events. The effect of this concatenated feedforward inhibition can be observed in the lower right panel of Fig. 3, which shows the model GC's membrane potential as a function of time and flash intensity. The dip caused by the fast transient AC's suppressive input is clearly visible, as is the appropriate intensity dependence of the remaining depolarization.

Spike event patterns generated by the model ganglion cell

Finally, transformation of the GC potential time course into a series of action potentials is accomplished by interpreting GC activation as a firing probability. Refractoriness, i.e. the reduced likelihood of a neuron eliciting many spikes in rapid succession, is accounted for by temporally lowering the basic firing probability each time a spike is fired (see Methods). This mechanism forces the spikes to be separated in time by a certain interval. As in the experiment, model spikes are generated for a number of stimulus repetitions. These are plotted in the lowermost left panel of Fig. 3. For comparison, the experimentally obtained spike trains are shown in this panel as well. The model spike trains correspond to their experimental counterparts, correctly reproducing both spike number and intensity dependent timing of the events. The analysis of spike train distances, described in detail in the Methods section, yields a difference of 0.10 standard deviations (sdv) between experimental and model spike trains for the ON part, and a difference of 1.25 sdv for the OFF part. Parameters of the inner retinal cells and the spike generation mechanism were adapted by minimizing the difference between the average instantaneous experimental and model firing rates (see Table 1 for the final inner retinal parameter values).

For flashes of high intensity, the inhibitory effect of the fast transient AC described above allows the model GC to generate action potentials only at the beginning and the end of the ON depolarization that arrives from the ON BC. Spikes in the first of these two events occur later with reduced intensity, copying the BC input's latency behavior. In contrast, spikes belonging to the second ON event occur earlier the less bright the flashes are, since both the BC input as well as the inhibition of the fast transient AC end earlier with decreasing intensity. This condition changes for intermediate intensities, when the fast transient AC is not sufficiently activated and therefore no longer interrupts the GC depolarization. At this point, the pause between first and second event is determined by the refractory period of action potential generation. Due to the reduced likelihood of spike generation immediately after the first event, the occurrence of the second event is pushed back in time, retaining a more or less fixed interval between the two events. The first event's latency increase for flashes of decreasing intensity therefore induces a corresponding shift towards longer latencies in the second event, which ultimately results in the second event's s-shaped timing. Thus, the experimentally observed behavior is reproduced in the model by a combination of two mechanisms: a direct inhibitory input from a fast transient amacrine cell at high intensities and refractoriness of spike generation at low intensities. Thereby, the model provides a possible explanation for the initially surprising non-monotonic intensity dependence of the second ON event.

Flicker experiments

Stimulation

In the next step, we checked whether distinct spike events also occur in paradigms that are closer to naturally encountered stimuli but still yield results comparable to those observed in the simple flash paradigm. We continued to use spatially homogeneous illumination, but omitted long dark periods in between flashes to avoid adaptation effects.

Table 1 Sets of model parameters for the reproduction of example ganglion cell responses to flash and flicker stimulation, and for the flicker experiment under strychnine application, together with the control condition before application of the drug. Grouping is according to outer retinal, inner retinal and spike generation parameters. Parameter values marked with a $^+$ symbol were not part of the fitting procedure and have been held fixed. * symbols indicate parameters being changed with respect to the previously fitted set presented to the left. Except for those of the photoreceptor, saturation parameters D_v and H_v are not included, since their values were fixed for all paradigms and are given in the Methods section

	Model neuron	Parameter symbol	Flash	Flicker	Pre-strychnine	Strychnine
Outer retina	PR	R	0.173	0.173	0.173	0.173
		I_0	0.0366	0.2928*	0.732*	0.732
		N	0.583	0.583	0.583	0.583
		τ	0.0105s	0.0105s	0.0105s	0.0105s
		Δt_s	0.003s	0.003s	0.003s	0.003s
		A_p	14.6/s	14.6/s	14.6/s	14.6/s
		D_p	2.82	2.82	2.82	2.82
		H_p	29.6	29.6	29.6	29.6
		W_p^h	2.5	2.5	2.5	2.5
		Δt_h	0.038s	0.038s	0.038s	0.038s
	HC	A_h	60.1/s	60.1/s	60.1/s	60.1/s
		W_h^p	0.2$^+$	0.2$^+$	0.2$^+$	0.2$^+$
Inner retina	BC	$A_{b\,ON}$	29.8/s	29.8/s	29.8/s	29.8/s
		$A_{b\,OFF}$	500/s$^+$	500/s$^+$	500/s$^+$	500/s$^+$
		W_b^p	1.0$^+$	1.0$^+$	1.0$^+$	1.0$^+$
		$W_{b\,ON}^{a\,S\,ON}$	68.4	68.4	68.4	68.4
		$W_{b\,OFF}^{a\,S\,OFF}$	77.9	77.9	77.9	77.9
		Δt_{ON}	0.016s	0.025s*	0.025s	0.025s
		Δt_{OFF}	0.0s$^+$	0.012s^{+*}	0.012s$^+$	0.012s$^+$
	AC_{su}	$A_{a\,S\,ON}$	1.36/s	0.65/s*	0.65/s	0.65/s
		$A_{a\,S\,OFF}$	8.57/s	8.57/s	8.57/s	8.57/s
		$W_{a\,S}^b$	1.0$^+$	1.0$^+$	1.0$^+$	1.0$^+$
	AC_{str}	$A_{a\,ST\,ONOFF}$	0.1/s	0.1/s	0.1/s	0.1/s
		$W_{a\,ST\,ONOFF}^{b\,ON}$	1000$^+$	1000$^+$	1000$^+$	1000$^+$
		$W_{a\,ST\,ONOFF}^{b\,OFF}$	6920$^+$	6920$^+$	6920$^+$	6920$^+$
	AC_{ftr}	$A_{a\,FT\,ONOFF}$	511/s	50/s*	30/s*	30/s
		$W_{a\,FT\,ONOFF}^{b\,ON}$	4.06	4.06	4.06	4.06
		$W_{a\,FT\,ONOFF}^{b\,OFF}$	28.1	28.1	28.1	28.1
		$W_{a\,FT\,ONOFF}^{a\,ST\,ONOFF}$	28.7	33.0*	33.0	16.0*
	GC	A_g	500/s$^+$	500/s$^+$	500/s$^+$	500/s$^+$
		$W_g^{b\,ON}$	1.0$^+$	1.0$^+$	1.0$^+$	1.0$^+$
		$W_g^{b\,OFF}$	6.92$^+$	6.92$^+$	6.92$^+$	6.92$^+$
		$W_g^{a\,FT\,ONOFF}$	17.1	25.0*	25.0	25.0
Spike generation	GC	G	34.9	10.0*	10.0	10.0
		F	25.3	25.3	25.3	25.3
		τ_θ	7.80s	16.0s*	10.0s*	10.0s
		θ	0.0439	0.0439	0.0439	0.0439

Instead, stimuli were now pseudo-random sequences of intensities, with abrupt changes occurring every second. We refer to this stimulation paradigm as "slow flicker". The range from which intensities were chosen was larger than for the flash experiments; the minimum relative intensity was in this case 2^{-16} (4.8 log). Stimulus sequences contained all possible transitions from both the maximum and the minimum intensity to each intermediate intensity equally often, but with their order randomized.

To facilitate comparison with the results obtained in the flash experiments, single ganglion cell spike trains were sorted according to four different transition conditions, explained in the Methods section. The first sorting yields raster plots that show the cell's ON responses for different intensities. The second condition consists of transitions from lower to the maximum intensity and therefore also shows the cell's ON responses. Selecting the spike train slices for the third condition that share the minimum intensity as their end intensity necessarily yields OFF responses. Finally, the fourth condition combines all transitions with the maximum intensity as their start.

Ganglion cell responses to flicker stimulation

Taken together, the second and fourth conditions describe the cell's response to a "dark flash", a temporary decrease from a bright background intensity, while the first and third conditions correspond to onset and offset of flashes of different intensities, analogous to the flash experiments described above. As is shown in Fig. 4, response patterns in

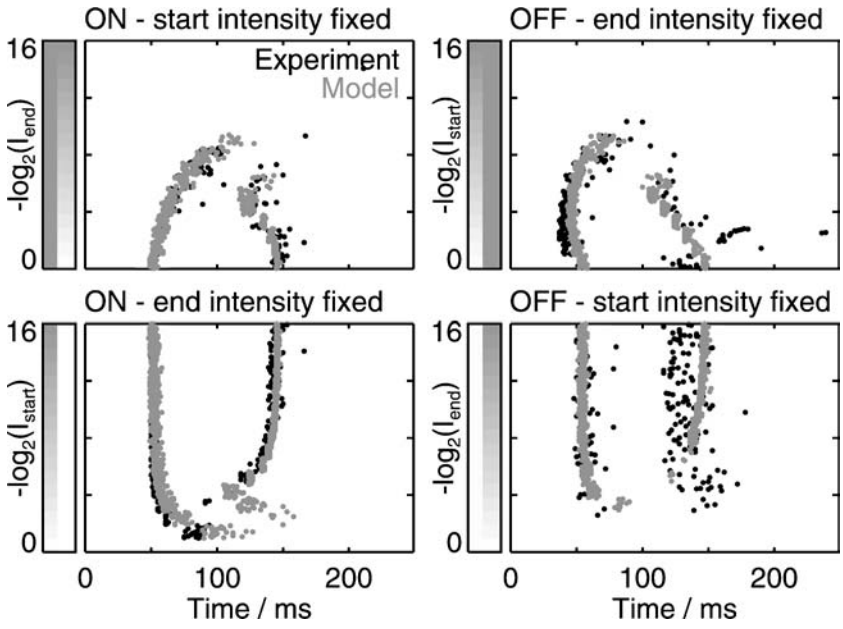

Fig. 4 Black dots: Action potentials of a ganglion cell in response to slow flicker stimulation with abrupt intensity changes every 1000 ms. Spike trains were aligned to the time of intensity change at time 0 and sorted according to four conditions, with the intensity either before or after the change held fixed. Each intensity step was presented repeatedly within the flicker sequence ($n = 28$). Intensity changes are indicated as grayscale boxes next to the spike rasters. Gray dots: spike responses to an identical stimulation computed with the cellular model of retinal processing

these conditions indeed look similar to the ON and OFF flash event patterns, indicating that adaptation plays only a minor role in their generation. In condition "ON—start intensity fixed", two spike events are clearly visible, with their latencies showing the same intensity dependence as the ON events known from the flash stimulation, namely decreasing latency of the first event and s-shaped latency of the second event with increasing end intensity. The ganglion cell's response for the OFF condition with fixed end intensity looks similar to the flash experiment as well, displaying a c-shaped intensity dependence of the first event. Responses to conditions two and four are characterized by nearly constant latency of the first event. However, for low contrast transitions, a small increase in the latency can be observed. Thus, the ON response not only depends on the present but also on the previous intensity, since otherwise the latency would always be the same in condition two. Spikes in condition four are strongly dispersed temporally, but two events can still be distinguished, whereas spike times in condition two are conserved across trials, yielding two distinct events, the second of which occurs earlier with increasing start intensity.

Responses of the cellular retina model

We simulated the response of the cellular model's ganglion cell to a stimulus identical to the slow flicker used in the experiments. Sequences of stimulus transitions were randomly generated, fed into the model as a continuous time course, and the simulated spikes were sorted afterwards in the same manner as the experimental data. In this way, possible influences of stimulus history on model responses due to long lasting processes are similar to the experiments.

Figure 4 shows the cellular model's spikes in relation to a real ganglion cell's action potentials for the four stimulus conditions. The timing of model spikes generally agrees well with experimental results. Spike train distance analysis yields a difference of 0.05 sdv for condition one, 0.04 sdv for condition two, 0.22 sdv for condition three, and 0.44 sdv for condition four. The higher average intensity of the flicker stimulus compared to the flash paradigm and the resulting change in the retina's adaptational state required adjustment of eight parameters with respect to the set obtained from the flash experiments. For instance, the latency of the second ON event is 30 ms longer in the GC shown as an example from the slow flicker experiments. This required a reduction of the sustained and the fast transient AC's membrane decay rates $A_{aS\,ON}$ and $A_{aFT\,ONOFF}$. For the outer retinal parameters, only I_0 of the PR's compressing nonlinearity had to be changed (see Table 1 for the list of parameter values chosen to reproduce the flicker experiments).

Spike patterns in conditions one and three show the intensity dependence already known from simulations of the flash experiments, since the same intra-retinal mechanisms are at work here. In conditions two and four, latency changes of the model's first event are restricted to low contrast transitions, while model spikes occur independent of the actual size of high contrast steps. This is also in accordance with the experimental results, although the model fails to reproduce the high temporal jitter of condition four. The constant latency for most intensity steps is both a consequence of the dual logarithmic choice of intensity steps and the nonlinear transduction in the PR. Intensity differences and, consequently, differences in latency as well are much smaller for the steps at the lower end of the stimulus range. However, without the

nonlinearity, latencies would be leveled across an even wider intensity range.

Effects of strychnine application

Description of strychnine experiments and model predictions

Since the critical part of the model is constituted by inhibitory amacrine cells, we tried to strengthen our assumptions about their interactions by pharmacologically interfering with inner retinal signal transduction. Most amacrine cells either release GABA or glycine as their neurotransmitter. Since blocking of GABAergic transmission would also affect outer retinal transmission, we had to choose the glycine receptor antagonist strychnine to block glycinergic synapses. Strychnine was added to the Ringer solution, and the retina was stimulated according to the slow flicker paradigm. After a period of 30 min, strychnine application was stopped and superfusion continued with the normal Ringer solution.

We used the model to predict possible effects of strychnine application depending on which type of amacrine cell would be affected. Strychnine is supposed to block the glycine receptors of the target cells, therefore any connection possibly affected should be either completely abolished or at least weakened. In the model, there are three effects that could occur; the corresponding connections are labeled by encircled numbers in the model schema in Fig. 2. Firstly, the weakening of inhibitory feedback of sustained ACs onto BCs (connection 1) would result in more sustained spiking in the ganglion cell for low intensities, which changes to a transient ON response at higher intensity steps. Secondly, decreasing the inhibition of the GC by the fast transient ON/OFF AC (connection 2) would result in a shorter interruption of the ON depolarization and therefore in a shorter interval between the first and the second ON event at high intensities, eventually destroying the second event's s-shaped latency behavior and leading qualitatively to a slow transient ON/OFF response. As a third possibility, weakening the inhibition of the fast transient ON/OFF AC by the slow transient AC (connection 3) would yield stronger inhibition of the GC, thereby strengthening and prolonging the interruption of the GC's ON depolarization, eventually leading to the complete disappearance of the second ON event's spikes and resulting in a fast transient ON/OFF response.

Comparison of experimental results and predictions

Figure 5 shows the effects of blocking glycinergic transmission on a ganglion cell's spike event pattern. Spike rasters are again arranged according to the four conditions of increasing and decreasing intensities with either start or end intensity fixed. The first column shows the cell's response prior to strychnine application. Before incubation, the typical event pattern can be observed, although in this cell's response, an additional spike event is present immediately after the first one in the ON conditions, copying the first event's latency dependence. Thus, in this example, the event displaying the characteristic s-shape in the first condition is the third event after the intensity step. Model parameters were initially adjusted for the spike patterns to match this experimental pre-strychnine control. In particular, to reproduce the second ON event, it was necessary to increase the fast transient AC's membrane time constant with respect to the value chosen previously. This allows more time for a second spike to occur before the GC potential is reduced (see Table 1 for complete parameter set). With these alterations, model spike trains for the pre-strychnine control closely resemble experimental results, with differences of 0.08 sdv, 0.76 sdv, 1.15 sdv, and 0.50 sdv for the four conditions according to the spike train distance analysis.

The second column of Fig. 5 represents spikes recorded during strychnine incubation, showing that application of the drug profoundly changes the event patterns. In all conditions, events two and three vanished, while the first event remained largely unaltered. The right column in Fig. 5 displays the control condition after washing out strychnine. Obviously, the drug-induced effects are reversible, with the cell's initial pattern restored after the wash.

The disappearance of all but the first spike event is consistent with the third of our predictions, namely that the inhibition of the fast transient ON/OFF AC by the slow transient type is reduced due to blocking glycinergic transmission. Gray dots in the second column of Fig. 5 show the successful reproduction of strychnine effects by the model. Spike train distance analysis for the model's strychnine predictions yields 0.12 sdv, 0.15 sdv, 0.25 sdv, and 0.17 sdv for conditions one to four. To obtain these responses, only a single model parameter, namely $W_{a\,FT\,ONOFF}^{a\,ST\,ONOFF}$ in Eq. (10), had to be changed. The reduced inhibition of the fast transient AC by the slow transient AC in turn increases the inhibitory effect of the fast transient AC onto the GC. Thereby, GC depolarization is suppressed earlier and suppression lasts longer, eliminating both the earlier second ON as well as the later third ON event.

Tracking strychnine effects during application

Closer inspection of the experimental results in Fig. 5 reveals that in the ON conditions, a part of the third event remains for intensity steps of low contrast. It seems that spikes in response to low contrast steps are either unaffected or possibly need higher strychnine concentrations to be eliminated. Due to diffusion, strychnine concentration in the retina preparation increases during application. As stimulation and recording continued after we started the application of the

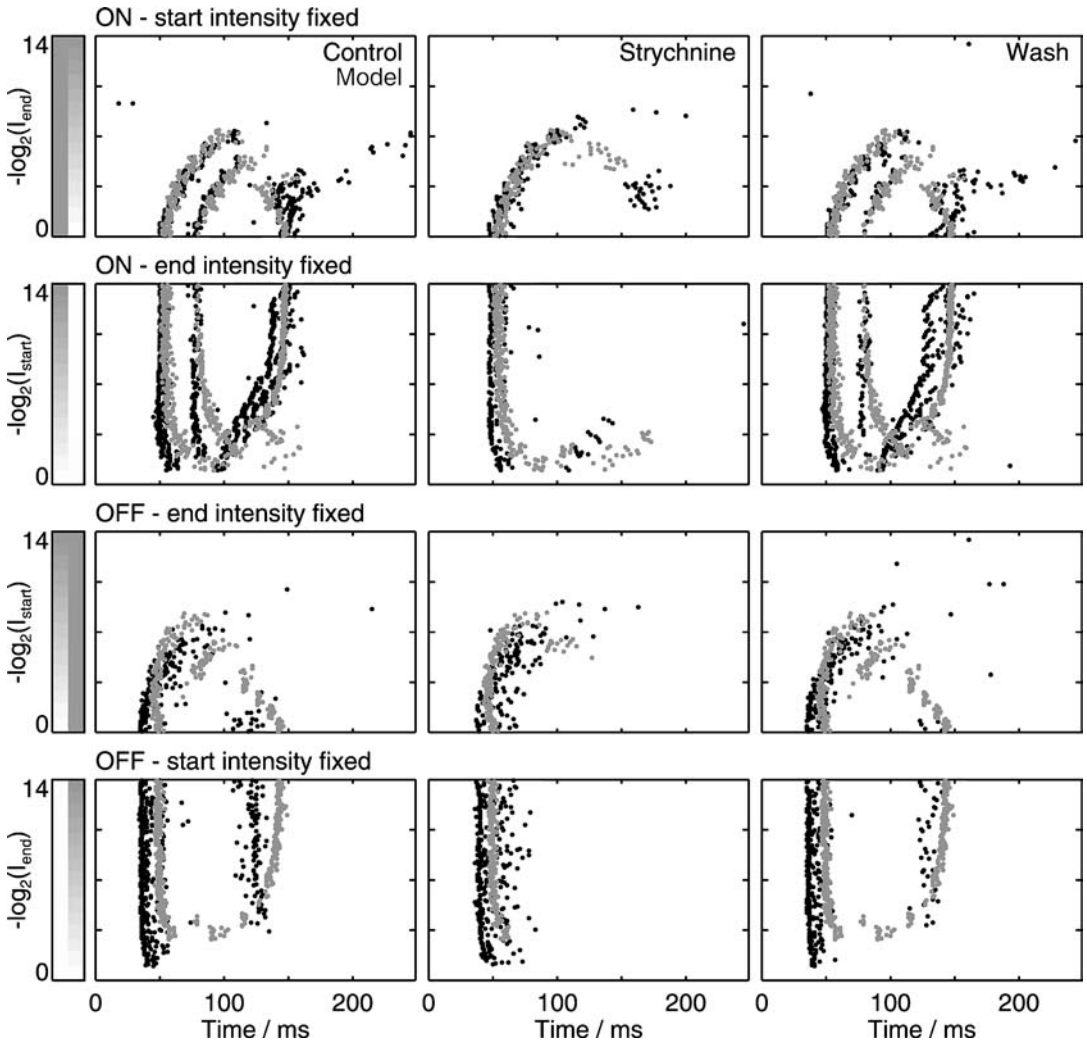

Fig. 5 Effects of strychnine application on the event patterns recorded in response to slow flicker stimulation. Black dots indicate spikes recorded from a ganglion cell, gray dots are computed using the cellular retina model. *Left column:* Responses before strychnine application for the four different conditions of intensity changes. *Middle column:* Response patterns during strychnine application. *Right column:* Control responses after washing strychnine from the superfusion liquid

drug, it was possible to monitor slight changes in the event patterns and thereby directly track the effects of glycinergic transmission gradually getting weaker.

These effects can best be exemplified in the temporal shift of spikes that belong to the third event in the ON condition with fixed end intensity. Since in this experiment we iterated the same sequence of intensity steps, which lasts approximately one minute, each single transition repeatedly occurred within an interval of one minute. In the top left panel of Fig. 6, we plotted spike trains in response to these repeatedly occurring identical intensity steps one below the other, with early traces first. The time since the start of strychnine application is represented in the gray level of the spike dots; the darker the dots are, the longer the incubation has already lasted. These sub-raster plots were again sorted according to the start intensity. This procedure yields a spike raster that reports changes in spike timing, which are due to slight increases in strychnine concentration in the retina during subsequent presentations of the same intensity step. In Fig. 6, the gradual increase in the late event's latency is evident as the darker dots are shifted towards later times. This is observed best for high start intensities in the lowermost part of the panel. Thus, it seems that strychnine does not simply eliminate the late ON event, but that spikes gradually disappear after being shifted to increasingly later times, starting with those elicited by large intensity steps.

Since we repeated the stimulus sequence 30 times, the last trial was measured after approximately 30 min of strychnine incubation. In the bottom two panels of Fig. 6, we plotted the time shift ΔT of the spikes in the last ON event as a function of strychnine incubation time. The lower left panel shows the spike shift for a low contrast transition, characterized by the presence of spikes even after half an hour of strychnine application. In contrast, the lower right panel shows that the

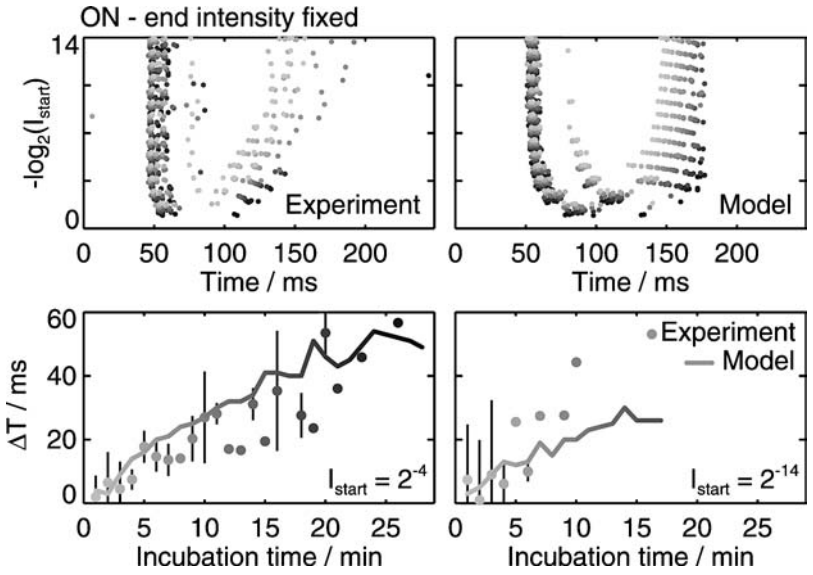

Fig. 6 *Top left:* Spikes of a ganglion cell recorded during 30 min of strychnine application for transitions that share the maximum end intensity, sorted according to the start intensity. Identical transitions are plotted one above another, with the time since the start of strychnine application represented in the gray scale of the spike dots; darker dots indicate longer incubation time. *Top right:* Model prediction for identical stimulation and gradual decrease of slow transient to fast transient ON/OFF AC coupling. *Bottom:* Timing ΔT of the last ON event relative to the time at which it occurred without pharmacological intervention as a function of strychnine incubation time for two different start intensities. Dots: experimental results averaged over five cells, with grayscale symbolizing the time since start of strychnine application. Bars indicate standard deviation of spike times. Shaded gray curves: predictions obtained from model computations

spikes of the last event disappear for high contrast transitions after about 10 min.

The raster in the top right panel and the curves in the two bottom panels of Fig. 6 show results obtained with the cellular retina model. By gradually reducing inhibition of the fast transient AC, it is possible to reproduce the observed shift of spike times quite accurately. Model stimulation was analogous to that used in the experiments, repeating the same sequence of intensity steps, while changing the model parameter $W_{a\,FT\,ONOFF}^{a\,ST\,ONOFF}$ at the beginning of each repetition. The effect of increasing strychnine concentration on the connection strength is described here by an exponential decrease as a function of time. The start and end values for this function are fixed by the parameters describing the weakest and strongest strychnine effects as shown in Fig. 5. Its time constant was chosen manually to minimize the discrepancy between the predicted and actual time shifts ΔT. For low contrast transitions, this works reasonably well (Fig. 6, lower left panel), while for the high contrast steps, the slope of the time shift is actually higher than the model prediction (Fig. 6, lower right panel). Thus, in addition to reproducing the disappearance of the second and third events, the model also correctly predicts both the gradual changes that lead to the final vanishing of events and the earlier disappearance of spikes for higher than for lower contrast transitions. In conclusion, the model's successful prediction of the strychnine effects, especially the reproduction of the late event's gradual latency increase, further supports our assumptions about the intra-retinal interactions generating temporally structured ganglion cell responses.

Discussion

Several detailed computational models have already been developed to investigate the interplay between intra-retinal physiological processes and ganglion cell responses. For instance, generation of synchronous oscillations in ganglion cells (Kenyon et al., 2003), various stages of light adaptation (Wilson, 1997), and nonlinear response characteristics of Y cells (Gaudiano, 1994; Hennig et al., 2002) have all been analyzed in this way. Complex cellular interactions in the inner retina have even been subject to neuromorphic replication (Zhagloul and Boahen, 2004). All these studies consistently found the delayed inhibition of bipolar cells by amacrine cells to be crucial for the transient response behavior of certain ganglion cell types. Additionally, this recurrent inhibition may be dynamically regulated by a different set of ACs, mutually coupled in a suppressive way to the first type (Hennig et al., 2002; Zhagloul and Boahen, 2004). In salamander, these cells have been anatomically identified as wide field amacrine cells, whereas those ACs that are responsible for the transient BC signal in the first place are regarded as narrow field (Roska et al., 1998). However, all these models mainly focus on spatial processing, and none has been applied to investigate the physiological

foundations of complex temporal structure in ganglion cell responses.

Teeters et al. (1997) proposed a model that is concerned with reproducing transient ON/OFF ganglion cell responses. It includes two types of amacrine cells: Narrow field ACs provide transient responses by delayed negative feedback onto bipolar cells, therefore corresponding to our AC_{su}, whereas wide field amacrines directly inhibit the model's ganglion cells, and thus are analogous to the fast transient AC of our model. In Teeters' simulations, wide field ACs are assumed to generate spikes. This nonlinear mechanism may be similar to the threshold effect in our fast transient AC, caused by the tonic input of slow transient AC. However, Teeters and coworkers did not analyze the temporal fine structure of ganglion cell responses as a function of intensity, they even refrained from generating spikes at all. Furthermore, we included a third type of AC as a counterbalance to the fast transient AC. In Teeters' model, wide field amacrine cell input therefore completely suppresses the late part of the transient ganglion cell activation, whereas our amacrine cell connections enable the GC potential to rise again at the end of the transient ON and OFF peaks, allowing for a second spike event.

In addition to these complex models, several attempts have been made to describe retinal function on a lower level of detail, one main approach being linear-nonlinear (LN) models. These models successfully describe ganglion cell responses to flicker stimuli by applying a single linear filter and a static nonlinear transfer function, in some cases followed by a spike generation mechanism (Keat et al., 2001). However, this technique is bound to fail in our case, since we are concerned with ON/OFF cells, which necessarily cannot be accurately described by a single linear filter. Even a modified two-dimensional LN model, combining two separate ON and OFF filter kernels, is unable to capture the spike events' temporal fine structure, both under fast and slow flicker stimulation, whereas we successfully reproduced spike event patterns using a cascade model, similar to the one proposed by van Hateren et al. (2002) for the magnocellular cells in macaque retina (Greschner, Thiel, Ammermüller; submitted). We were able to identify a fast divisive contrast gain control loop within the cascade model as the main nonlinear mechanism responsible for the temporal fine structure in spike activity, since it creates a dip of low spiking probability in the GC generator potential in between the two ON events. In the cellular model described here, this corresponds to the inhibitory effect of the fast transient AC upon the GC. The former may thus be thought of as realizing a form of contrast gain control, since it provides the GC potential with the major characteristics of this well known stage of retinal processing: Due to the inhibitory signal originating from the fast transient AC, large peaks in GC depolarization are shortened and reduced in size. This corresponds to a decreased time constant of the high pass filter in an early formulation of the contrast gain control mechanism (Victor, 1987), and to stronger feedback inhibition in later models (Berry et al., 1999; van Hateren et al., 2002). The nonlinearity that is part of these models in order to ensure that larger peaks are affected more strongly than small ones is realized in the cellular model by a form of threshold operation. Inhibition of the GC sets in only after the fast transient AC is sufficiently depolarized, which does not happen for small illuminance changes due to the tonic suppression originating from the slow transient AC. A major difference to the abovementioned contrast gain control models is that the AC inhibition used here allows the underlying GC activity to rise again at the end of an activity pulse, a prerequisite for the late spike events to occur.

With the cellular retina model described above, we succeeded in reproducing spike event patterns observed in different cells' responses under different stimulation paradigms. For all simulations presented here, the model's overall connectivity remained identical, and only minor parameter changes were necessary. Thus, in spite of the high number of free parameters, the model's agreement with the experimental data is unlikely to be obtained by overfitting. In particular, we were able to pin down the alterations in spike events observed after strychnine application to a single parameter change, and therefore to support our hypothesis about the generation of these events. For 12 out of 14 event patterns, the average spike train distance between model and experiment differed less than one standard deviation from the average dissimilarity between experimental spike trains. Moreover, PR and HC responses were correctly reproduced across a number of different flash intensities, and model amacrine cell responses were in qualitative accordance with intracellular recordings. All responses of amacrine cells that were not recorded in this study, namely sustained OFF and slow ON/OFF, have been described elsewhere (Marchiafava and Weiler, 1982; Ammermüller and Kolb, 1995, 1996). Moreover, the model connections are in excellent agreement with ultrastructural data of the basic wiring schemes in the inner retina. Reciprocal synapses between bipolars and amacrine cells correspond to connection 1, and in many cases a ganglion cell is postsynaptic in this triad arrangement (Guiloff et al., 1988). Also serial synapses BC-AC-AC and AC-AC-GC are regularly found in turtle and many other retinae (Dowling, 1987). The main difference between lower vertebrates and mammals is that amacrine cell involvement in synaptic circuitry is ubiquitous in the former, which corresponds to a higher number of transient ganglion cell types in these animals (Dowling, 1987). Clearly, ON/OFF ganglion cells in the turtle receive abundant bipolar cell input in both ON and OFF sublayers of the IPL, as well as GABAergic input from amacrine cells (Muller et al., 1991).

In those cases where specific data are lacking, parameter choices and properties of synaptic connections are motivated by the aim to construct a model that reproduces the particular set of experimental data presented here. Most notably, the decisions whether or not to crop the negative parts of presynaptic activity are solely based on modeling arguments, which are elaborated in the Methods section. These different modes of transmission from the same BC to various types of ACs are in fact difficult to justify if one assumes that they are purely caused presynaptically. However, half-wave rectification of BC activity may as well originate from postsynaptic mechanisms, like low transmitter binding affinity, different types of receptors and/or reversal potentials. These would reflect in the model as modified saturation levels D and H for the various amacrine cells, implying a further increase of unknown parameters. Thus, for the sake of simplicity, we decided to just crop the negative parts of presynaptic activity for certain cellular connections, although we do not claim that this corresponds to a mechanism with an exclusively presynaptic origin.

Naturally, the model's behavior is altered by modifying its parameters. Next, we will consider two possible types of such modifications and their consequences on model performance. On the one hand, major alterations, like changing the overall connectivity of bipolar- and amacrine cells by setting coupling strength parameters to zero, result in qualitative changes of the model ganglion cell's response type. On the other hand, fine tuning may be performed by small changes in the parameter set to account for the experimentally recorded cells' slightly different responses due to switching the experimental paradigm from flash to flicker and due to inherent variability between cells of the same type.

Considering parameter fine tuning, changes in the outer retina were restricted to I_0, the half maximum response of the photoreceptors, being especially profound for the transition from flash to flicker stimulation. Since intensity response curves shift towards higher intensities with light adaptation (Normann and Perlman, 1979a), the variation of the average intensity and the corresponding change in the retina's adaptational state is likely to be responsible for this modification. With increase in I_0, the sustained responses of PRs and HCs are shortened, in accordance with experimental results from PRs and HCs (Normann and Perlman, 1979a; Itzhaki and Perlman, 1984). Consequently, the depolarization in OFF bipolar cells after light offset occurs earlier. In the inner retina, the main modification needed to transform flash to flicker responses is a reduction of the membrane decay rates of AC_{su} and *ONOFF* AC_{ftr}. This slows down the responses of these cells, which in turn prolongs the responses of the ON BC, resulting in an increase in the last ON spike event's latency of about 50 ms. The change in membrane decay rates of the putative GABAergic amacrine cells possibly reflects additional adaptational effects via the dopaminergic system in the turtle inner retina interacting with the GABAergic system (Netzer et al., 1997). In contrast, parameter changes that are necessary to bring the model cell into accordance with the experimental response prior to strychnine application are smaller and less numerous than those for the transition from flash to flicker (compare Figs. 4 and 5, and Table 1, respectively). Namely generating three instead of two ON bursts needed only inner retinal parameter adjustments, emphasizing the role of the inner retina in producing the temporal response structure.

Although originally developed to reproduce the intensity dependence of the various spike events in fast transient ON/OFF ganglion cells, the model might represent a basic wiring module for radial processing in the retina, generally capable of reproducing most experimentally observed ganglion cell response types in the turtle (Bowling, 1980; Jensen and DeVoe, 1982; Kittila and Granda, 1994; Ammermüller and Kolb, 1995, 1996). In contrast to the quantitative parameter changes necessary to fine tune the model, all basic response types of ganglion cells such as sustained ON, sustained OFF, transient ON, and ON/OFF can be obtained within the model framework by switching off certain inner retinal connections by setting their coupling strength parameters to be zero. This has been shown for omission of connection 3 (Fig. 2), with the response type changing to pure fast transient ON/OFF in the strychnine modeling. Blocking connection 2 in the model yields qualitatively a slow transient ON/OFF response, which is also well known in turtle ganglion cells. A transient ON response can be obtained by exclusively removing connection 1. Vigh and Witkovsky (2004) report that turtle ON/OFF ganglion cell responses become less transient or even sustained in the presence of GABA blockers, which is reproduced by the model if both connections 1 and 2 are weakened. Restricting ganglion cell input to either from ON or OFF bipolar cells and again blocking connections 1 and 2 results in sustained either ON or OFF responses.

These model variations based on different wiring schemes may give a hint to why so many different types of bipolar, amacrine, and ganglion cells are present in the retina. Necessarily, the bipolar cells receiving reciprocal input from amacrine cells at their terminal have to differ from those without reciprocal input (Masland, 2001a, 2001b). Taking into account the ON/OFF subdivision results in at least four types of bipolar cells needed in the luminosity pathways. In the case of amacrine cell diversity, our model postulates at least four different types, again taking the ON/OFF subdivision into account. Spatial aspects will play an additional role, which were not studied here. Nevertheless, at least two types of glycinergic amacrine cells have been described in the turtle retina (Eldred and Cheung, 1989; Weiler et al., 1991), and about 50 percent of the glycine receptors have been shown to be localized on amacrine cell dendrites; thus connection 3

is very likely to exist in reality (Zucker and Ehinger, 1993). One of the glycinergic AC types is probably small field and a candidate for the model's slow transient ON/OFF cell. The other type is wide field, possibly subserving spatial functions described by Hennig et al. (2002). We suggest that the fast ON/OFF amacrine cell is probably GABAergic, based on the fact that the feedforward inhibition of connection 2 still has to work in order to explain the strychnine results.

The model suggests a possible functional role for the typical, highly conserved wiring schemes of reciprocal and concatenated suppression. Obviously, the inner retinal inhibitory circuitry is responsible for the transformation of intensity changes into a series of distinct spike events. The systematic stimulus dependence and the precisely reproducible timing of those events are prerequisites for temporal coding (Berry et al., 1997; Berry and Meister, 1998). Indeed, we succeeded in reliably categorizing intensity steps using the temporal structure of the spike events, and found that inclusion of the second event improved stimulus estimation (Greschner, Thiel, Ammermüller; submitted). The question arises as to what function ON/OFF ganglion cells have in the retina, beyond the well-studied directional selectivity. The response pattern of the transient ON/OFF type studied here is rather robust in terms of interference by spatial stimulus configuration, being observed equally well when stimulating with small spots or moving gratings (Greschner, Thiel, Ammermüller; submitted). This is not the case for sustained ON or OFF cells, where the response largely depends on the spatial configuration of a stimulus (Ammermüller and Kolb, 1995, 1996). Combining the responses of sustained ON and OFF cells with those of the presented ON/OFF type could possibly reduce or solve the ambiguities contained in the single cell responses by using a combinatorial code. Redundancies as large as 14% have been shown to occur among nearby ganglion cells in the retina, suggesting that some advantages should exist underlying this neuronal overrepresentation (Puchalla et al., 2005).

Acknowledgments We thank Malte T. Ahlers for constructing the programmable LED stimulation system and Jennifer Shelley for critical reading of the manuscript. This work was supported by grants of the European Community (CORTIVIS) and the Deutsche Forschungsgemeinschaft (AM 70/10) to J.A.

References

Ammermüller J, Kolb H (1995) The organization of the turtle inner retina. I. ON and OFF-center pathways. J. Comp. Neurol. 358: 1–34.

Ammermüller J, Muller J, Kolb H (1995) The organization of the turtle inner retina. II. Analysis of color-coded and directionally selective cells. J. Comp. Neurol. 358: 35–62.

Ammermüller J, Kolb H (1996) Functional architecture of the turtle retina. Prog. Retin. Eye Res. 15: 393–433.

Ariel M, Daw NW, Rader RK (1983) Rhythmicity in rabbit retinal ganglion cell responses. Vision Res. 23: 1485–1493.

Awatramani GB, Slaughter MM (2000) Origin of transient and sustained responses in ganglion cells of the retina. J. Neurosci. 20: 7087–7095.

Belgum JH, Dvorak DR, McReynolds JS (1982) Sustained synaptic input to ganglion cells of mudpuppy retina. J. Physiol. 326: 91–108.

Belgum JH, Dvorak DR, McReynolds JS (1983) Sustained and transient synaptic inputs to ON – OFF ganglion cells in the mudpuppy retina. J. Physiol. 340: 599–610.

Belgum JH, Dvorak DR, McReynolds JS (1984) Strychnine blocks transient but not sustained inhibition in mudpuppy retinal ganglion cells. J. Physiol. 354: 273–286.

Berry MJ, Brivanlou IH, Jordan TA, Meister M (1999) Anticipation of moving stimuli by the retina. Nature 398: 334–338.

Berry MJ, Warland DK, Meister M (1997) The structure and precision of retinal spike trains. Proc. Natl. Acad. Sci. USA 94: 5411–5416.

Berry MJ, Meister M (1998) Refractoriness and neural precision. J. Neurosci. 18: 2200–2211.

Bowling DB (1980) Light response of ganglion cells in the retina of the turtle. J. Physiol. 299: 173–196.

Burns ME, Lamb TD (2003) Visual transduction by rod and cone photoreceptors. In: LM Chalupa, JH Werner, eds. Visual Neurosciences. MIT Press, Cambridge, MA, pp. 215–233.

Cajal SR y (1892) The structure of the retina (Thorpe SA and Glickstein M, trans 1972) Thomas, Springfield, IL.

Dearworth JR, Granda AM (2002) Multiplied functions unify shapes of ganglion-cell receptive fields in retina of turtle. J. Vis. 2: 204–217.

Dowling JE (1987) The retina: An approachable part of the brain. Belknapp Press, Cambridge, MA.

Eckhorn R, Reitboeck HJ, Arndt M, Dicke P (1990) Feature linking via synchronization among distributed assemblies: Simulations of results from cat visual cortex. Neural Comput. 2: 293–307.

Eldred WD, Cheung K (1989) Immunocytochemical localization of glycine in the retina of the turtle (Pseudemys scripta). Vis. Neurosci. 2: 331–338.

Flannery BP, Teukolski SA, Press WH, Vettering WT (1993) Numerical recipes in C. Cambridge UP, Cambridge, MA.

Gaudiano P (1994) Simulations of X and Y retinal ganglion cell behavior with a nonlinear push-pull model of spatiotemporal retinal processing. Vision Res. 34: 1767–1784.

Golcich MA, Morgan IG, Dvorak DR (1990) Selective abolition of OFF-responses in kainic acid-lesioned chicken retina. Brain Res. 535: 288–300.

Granda AM, Fulbrook JE (1989) Classification of turtle retinal ganglion cells. J. Neurophysiol. 62: 723–737.

Guiloff GD, Jones J, Kolb H (1988) Organization of the inner plexiform layer of the turtle retina: An electron microscopic study. J. Comp. Neurol. 272: 280–292.

Hennig MH, Funke K (2001) A biophysically realistic simulation of the vertebrate retina. Neurocomputing 38–40: 659–665.

Hennig MH, Funke K, Wörgötter F (2002) The influence of different retinal subcircuits on the nonlinearity of ganglion cell behavior. J. Neurosci. 22: 8726–8738.

Itzhaki A, Perlman I (1984) Light adaptation in luminosity horizontal cells in the turtle retina. Vision Res. 24: 1119–1126.

Jensen RJ, DeVoe RD (1982) Ganglion cells and (dye-coupled) amacrine cells in the turtle retina that have possible synaptic connection. Brain Res. 240: 146–150.

Keat J, Reinagel P, Reid RC, Meister M (2001) Predicting every spike: A model for the responses of visual neurons. Neuron 30: 803–817.

Kenyon GT, Moore B, Jeffs J, Denning KS, Stephens GJ, Travis BJ, George JS, Theiler J, Marshak DW (2003) A model of high-freqeuncy oscillatory potentials in retinal ganglion cells. Vis. Neurosci. 20: 465–480.

Kittila CA, Granda AM (1994) Functional morphologies of retinal ganglion cells in the turtle. J. Comp. Neurol. 350: 623–645.
Lukasiewicz PD, Werblin FS (1990) The spatial distribution of excitatory and inhibitory inputs to ganglion cell dendrites in the tiger salamander retina. J. Neurosci. 10: 210–221.
Lukasiewicz PD, Lawrence JE, Valentino TL (1995) Desensitizing glutamate receptors shape excitatory synaptic inputs to tiger salamander retinal ganglion cells. J. Neurosci. 15: 6189–6199.
MacNeil MA, Masland RH (1998) Extreme diversity among amacrine cells: implications for function. Neuron 20: 971–982.
Maguire G, Lukasiewicz PD, Werblin FS (1989) Amacrine cell interactions underlying the response to change in the tiger salamander retina. J. Neurosci. 10: 210–221.
Mainen ZF, Sejnowski TJ (1995) Reliability of spike timing in neocortical neurons. Science 268: 1503–1506.
Marchiafava PL (1979) The responses of retinal ganglion cells to stationary and moving visual stimuli. Vision Res. 19: 1203–1211.
Marchiafava PL, Weiler R (1982) The photoresponses of structurally identified amacrine cells in the turtle retina. Proc. Royal Soc. London B 214: 403–415.
Masland RH (2001a) Neuronal diversity in the retina. Curr. Opin. Neurobiol. 11: 431–436.
Masland RH (2001b) The fundamental plan of the retina. Nat. Neurosci. 4: 877–886.
Miller RF (1979) The neuronal basis of ganglion cell receptive field organization and the physiology of amacrine cells. In: FO Schmitt, FG Worden, eds. The Neuroscience, Fourth Study Program. MIT Press, Cambridge, MA. pp. 227–245.
Miller RF, Dacheux RF (1976) Synaptic organization and ionic basis of ON and OFF channels in the mudpuppy retina. III. A model of ganglion cell receptive field organization based on chloride-free experiments. J. Gen. Physiol. 67: 679–690.
Morgan IG (1992) What do amacrine cells do? Prog. Retin. Res. 11: 193–214.
Muller JF, Ammermüller J, Normann RA, Kolb H (1991) Synaptic inputs to physiologically defined turtle retinal ganglion cells. Vis. Neurosci. 7: 409–429.
Müller F, Kaupp UB (1998) Signaltransduktion in Sehzellen. Naturwissenschaften 85: 49–61.
Netzer E, DeKorver L, Ammermüller J, Kolb H (1997) Neural circuitry and light responses of the dopamine amacrine cell in the turtle retina. Mol. Vis. 3: 6–12.
Nirenberg S, Meister M (1997) The light response of retinal ganglion cells is truncated by a displaced amacrine cell circuit. Neuron 18: 637–650.
Normann RA, Perlman I (1979a) The effect of background illumination on the photoresponses of red and green cones. J. Physiol. 286: 491–507.
Normann RA, Perlman I (1979b) Signal transmission from red cones to horizontal cells in the turtle retina. J. Physiol. 286: 509–524.
Puchalla JL, Schneidmann E, Harris RA, Berry MJ (2005) Redundancy in the population code of the retina. Neuron 46: 493–504.
Roska B, Nemeth E, Werblin F (1998) Response to change is facilitated by a three-neuron disinhibitory pathway in the tiger salamander retina. J. Neurosci. 18: 3451–3459.
Sakai HM, Naka K-I (1987a) Signal transmission in the catfish retina. IV. Transmission to ganglion cells. J. Neurophysiol. 58: 1307–1328.
Sakai HM, Naka K-I (1987b) Signal transmission in the catfish retina. V. Sensitivity and circuit. J. Neurophysiol. 58: 1329–1350.
Sakai HM, Naka K-I (1988) Neuron network in catfish retina. Prog. Retin. Res. 7: 149–208.
Schwartz EA (1973) Organization of ON-OFF cells in the retina of the turtle. J. Physiol. 230: 1–14.
Sestokas AK, Lehmkuhle S, Kratz KE (1991) Relationship between response latency and amplitude for ganglion and geniculate X- and Y-cells in the cat. Int. J. Neurosci. 60: 59–64.
Teeters J, Jacobs A, Werblin F (1997) How neural interactions form neural responses in the salamander retina. J. Comput. Neurosci. 4: 5–27.
Toyoda J, Hashimoto H, Ohtsu K (1973) Bipolar-amacrine transmission in the carp retina. Vision Res. 13: 295–307.
van Hateren JH (1997) Processing of natural time series of intensities by the visual system of the blowfly. Vision Res. 37: 3407–3416.
van Hateren JH, Rüttiger L, Sun H, Lee BB (2002) Processing of natural temporal stimuli by macaque retinal ganglion cells. J. Neurosci. 22: 9945–9960.
Victor JD (1987) The dynamics of the cat retinal X cell centre. J. Physiol. 386: 219–246.
Victor JD, Purpura KP (1996) Nature and precision of temporal coding in visual cortex: A metric-space analysis. J. Neurophysiol. 76: 1310–1326.
Vigh J, Witkovsky P (2004) Neurotransmitter actions on transient amacrine and ganglion cells of the turtle retina. Vis. Neurosci. 21: 1–11.
Werblin FS, Dowling JE (1969) Organization of the retina of the mudpuppy, Necturus maculosus. II. Intracellular recording. J. Neurophysiol. 32: 339–355.
Werblin FS (1977) Regenerative amacrine cell depolarization and the formation of ON – OFF ganglion cell response. J. Physiol. 264: 767–785.
Werblin FS, Maguire G, Lukasiewicz PD, Eliasof S, Wu SM (1988) Neural interactions mediating the detection of motion in the retina of the tiger salamander. Vis. Neurosci. 1: 317–329.
Weiler R, Ball AK, Ammermüller J (1991) Neurotransmitter systems in the turtle retina. Prog. Retin. Res. 10: 1–26.
Wilson HR (1997) A neural model of foveal light adaptation and afterimage formation. Vis. Neurosci. 14: 403–423.
Zhagloul KA, Boahen K (2004) Optic nerve signals in a neuromorphic chip I: outer and inner retina models. IEEE Trans. Bio-Med. Eng. 51: 657–666.
Zucker CL, Ehinger B (1993) Synaptic connections involving immunoreactive glycine receptors in the turtle retina. Vis. Neurosci. 10: 907–914.